



STRUCTURAL BIOLOGY

Phosphorylation-dependent recognition of diverse protein targets by the cryptic GK domain of MAGI MAGUKs

Meng Zhang^{1,2†}, Aili Cao^{3,4†}, Lin Lin^{1†}, Ying Chen⁴, Yuan Shang⁵, Chao Wang², Mingjie Zhang⁶, Jinwei Zhu^{1*}

Dynamic signal transduction requires the rapid assembly and disassembly of signaling complexes, often mediated by phosphoprotein binding modules. The guanylate kinase-like (GK) domain of the membrane-associated guanylate kinases (MAGUKs) is such a module orchestrating signaling at cellular junctions. The MAGI subfamily of MAGUKs contains a truncated GK domain with unknown structure and function, although they participate in diverse physiological and pathological processes. Here, we demonstrate that the truncated GK domain of MAGI2 interacts with its adjacent PDZ0 domain to form a structural supramodule capable of recognizing phosphoproteins. A conserved phosphorylation-dependent binding motif for PDZ0-GK is delineated, which leads to identification of a set of previously unknown binding partners. We explore the structure and function of the MAGI2-target complex with an inhibitory peptide derived from the consensus motif. Our work reveals an action mechanism of the cryptic MAGI GKs and broadens our understanding of the target recognition rules of phosphoprotein binding modules.

INTRODUCTION

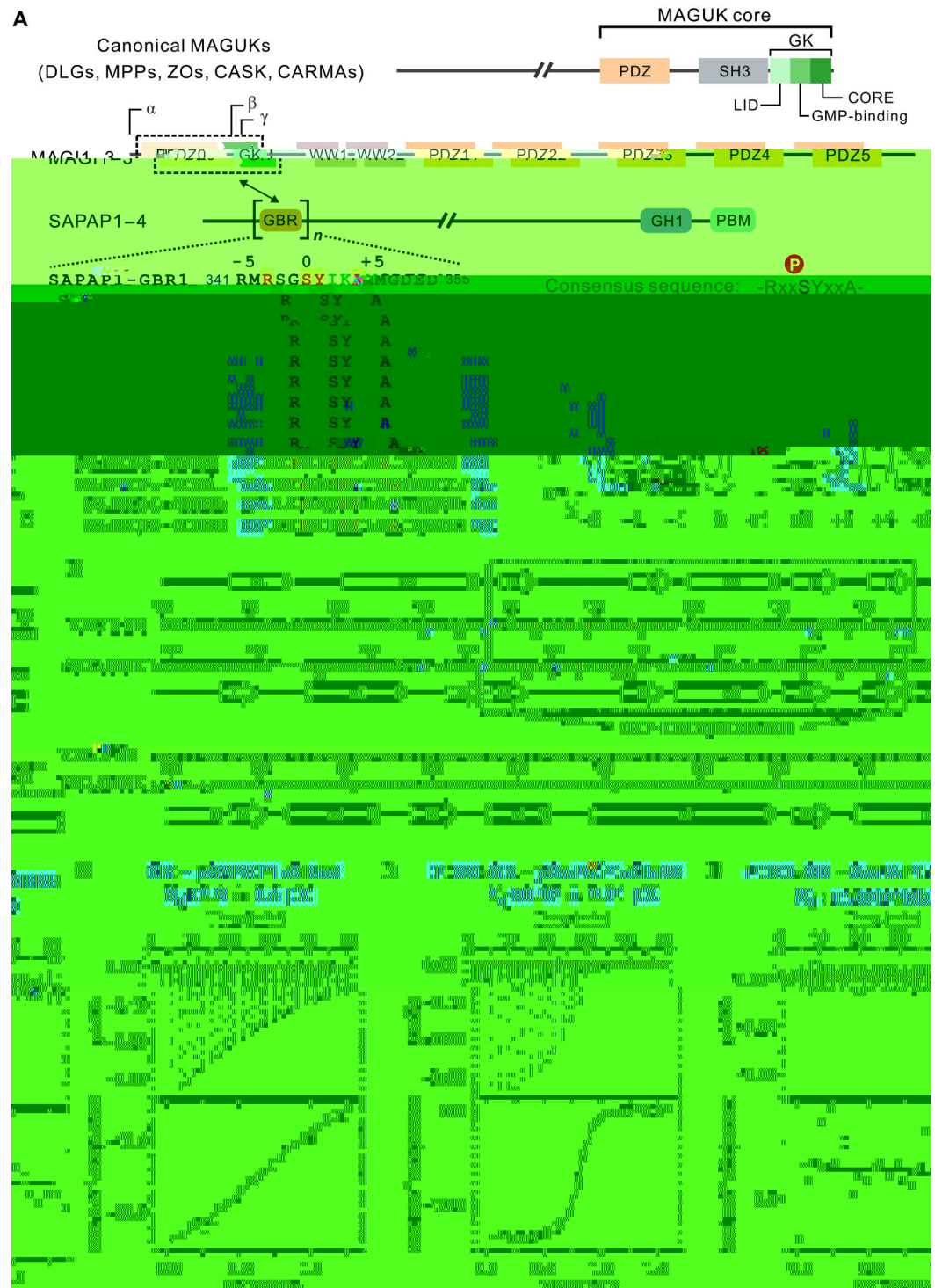
Membrane-associated scaffold proteins are crucial for spatiotemporal integration of intracellular signaling pathways in response to external stimuli. Membrane-associated guanylate kinases (MAGUKs) are such a family of multidomain scaffold proteins that orchestrate cortical signaling at various cellular junctions such as epithelial cell junctions and neuronal synapses (1, 2). They connect transmembrane proteins to cytosolic signaling complexes and cytoskeletal components through multiple protein-protein interaction modules (3).

A common fea

Copyright © 2023 The Authors, some rights reserved; exclusive licensee American Association for the Advancement of Science. No claim to original U.S. Government Works. Distributed under a Creative Commons Attribution NonCommercial License 4.0 (CC BY-NC).

Fig. 1. The PDZ0-GK tandem of MAGI2 specifically interacts with phosphorylated peptides from SAPAPs. (A) Schematic diagram of the domain organization of canonical MAGUKs, MAGIs, and SAPAPs. The interaction between MAGI and SAPAP is indicated by a two-way arrow. The MAGUK core is composed of the PDZ, SH3, and GK domains. The typical GK domain consists of the LID, CORE, and GMP-binding subdomains. The sequence alignment of the GBR of human SAPAPs is shown, with the absolutely conserved and conserved residues colored in red and green, respectively. The consensus motif derived from SAPAPs is shown, with the phosphorylation site annotated as Ser⁰. A sequence logo representing enriched residues within the consensus motifs from SAPAPs is also shown, generated using WebLogo (40). GH1, GKAP homology domain 1; PBM, PDZ-binding motif. Of note, there are three alternative splicing variants of the *MAGI2* gene: *MAGI2* α , *MAGI2* β , and *MAGI2* γ .

(B) Structure-based sequence alignment of the GK domain from *MAGI2* and PSD-95. In this alignment, the absolutely conserved and conserved residues are colored in red and green, respectively. Residues of *MAGI2* GK and PSD-95 GK that are involved in the recognition of phosphopeptides are annotated below as blue dots and purple dots, respectively. (C to E) ITC-based measurements of the binding affinities between *MAGI2* GK and pSAPAP1-GBR2 (C), *MAGI2* PDZ0-GK and pSAPAP1-GBR2 (D), and *MAGI2* PDZ0-GK and SAPAP1-GBR2 (E). The thermodynamic parameters of ITC assays were listed in table S2.



development and plasticity, and are associated with autism, obsessive-compulsive disorder, and schizophrenia (7, 16–18).

In the kidney, *MAGI2* is a key component of the slit diaphragm, a highly specialized cell junction between neighboring podocytes that functions as the final filtration barrier to prevent passage of proteins from the capillary lumen into the urinary space (19, 20). At the slit diaphragm, *MAGI2* associates with Nephryn, the defining

adhesion molecule, via its PDZ domains, serving as a bridge between the cortical membrane and cytosolic proteins (21, 22). Podocyte-specific *MAGI2* knockout mice displayed disruption of the slit diaphragm and progressive proteinuria (23). Moreover, mutations of *MAGI2* have been identified in patients with steroid-resistant nephrotic syndrome, with some of them occurring in the GK domain (24, 25), implying that dysfunction of the downstream

signaling mediated by MAGI2 GK may contribute to the etiology of nephrotic syndrome.

Despite the critical physiological and pathological roles of MAGI2 in both brain and kidney, the molecular basis of signal transduction mediated by the cryptic GK domain of MAGI2 remains largely elusive. A deeper mechanistic understanding of how MAGI2 GK interacts with its cognate target(s) might provide valuable insights into its biological functions. In this work, we report an unexpected discovery that the truncated MAGI2 GK is able to bind to phosphoproteins, while PDZ0-GK tandem exhibits a ~50-fold increased binding affinity (~70 nM). The crystal structures of MAGI2 PDZ0-GK in complex with two phosphopeptides from SAPAP1 reveal an unexpected GK fold of MAGI2 GK. The PDZ0 and GK domains of MAGI2 couple tightly to form a structural supramodule that is essential for phosphopeptide recognition. A consensus binding motif for MAGI2 GK is deduced by the C)Jdnr

PDZ0-GK and Y(+1)/R(-3) from pSAPAP1-GBR2, which is in contrast to that observed at the PSD-95 GK/pSAPAP1-GBR2 interface where Y(+1)^{pSAPAP1-GBR2} forms two hydrogen bonds with E600^{PSD-95 GK} and T611^{PSD-95 GK}, and R(-3) forms electrostatic interactions with D545^{PSD-95 GK} and D629^{PSD-95 GK} (Fig. 2, C and D). Of note, the MAGI2 PDZ0-GK/pSAPAP1-GBR3 complex shares almost the same interface with that of the MAGI2 PDZ0-GK/pSAPAP1-GBR2 complex, with the exception of R(-2)^{pSAPAP1-GBR2} being replaced by S(-2)^{pSAPAP1-GBR3} at the phosphor-site (fig. S2C).

To verify whether the key residues involved in the interface are essential for the complex assembly, we made a series of mutations on both PDZ0-GK and pSAPAP1-GBR2 and evaluated their binding abilities using the ITC-based assay (Fig. 2E). Expectedly, mutations of key residues that contribute to the interface all impaired the interaction (Fig. 2E). Specifically, substitution of R143^{PDZ0-GK} with Ala completely abolished its binding to pSAPAP1-GBR2, most likely due to the weakened interaction network at the phosphor-site (Fig. 2C). Reciprocally, replacement of A(+4)^{pSAPAP1-GBR2} by Gln also diminished the interaction, probably due to disruption of the hydrophobic interactions (Fig. 2E).

All key residues at the interface are absolutely conserved in MAGI2 from different species (fig. S1), implying the indispensable

role of this phosphopeptide recognition surface during evolution. Moreover, these residues are also conserved among MAGI1 to MAGI3 (fig. S1), indicating that the PDZ0-GK tandem of MAGI1 and MAGI3 may also bind to phosphopeptides. In line with this analysis, we demonstrated that PDZ0-GK of MAGI1 and MAGI3 interacted with pSAPAP1-GBR2 with comparable K_d values of ~0.36 and 0.40 μM , respectively (fig. S3).

Critical role of PDZ0-GK intramolecular interaction for phosphopeptide recognition

Since the phosphopeptide residue μM , co1q3FREq(C)Jdo9line 5JRj ofFO

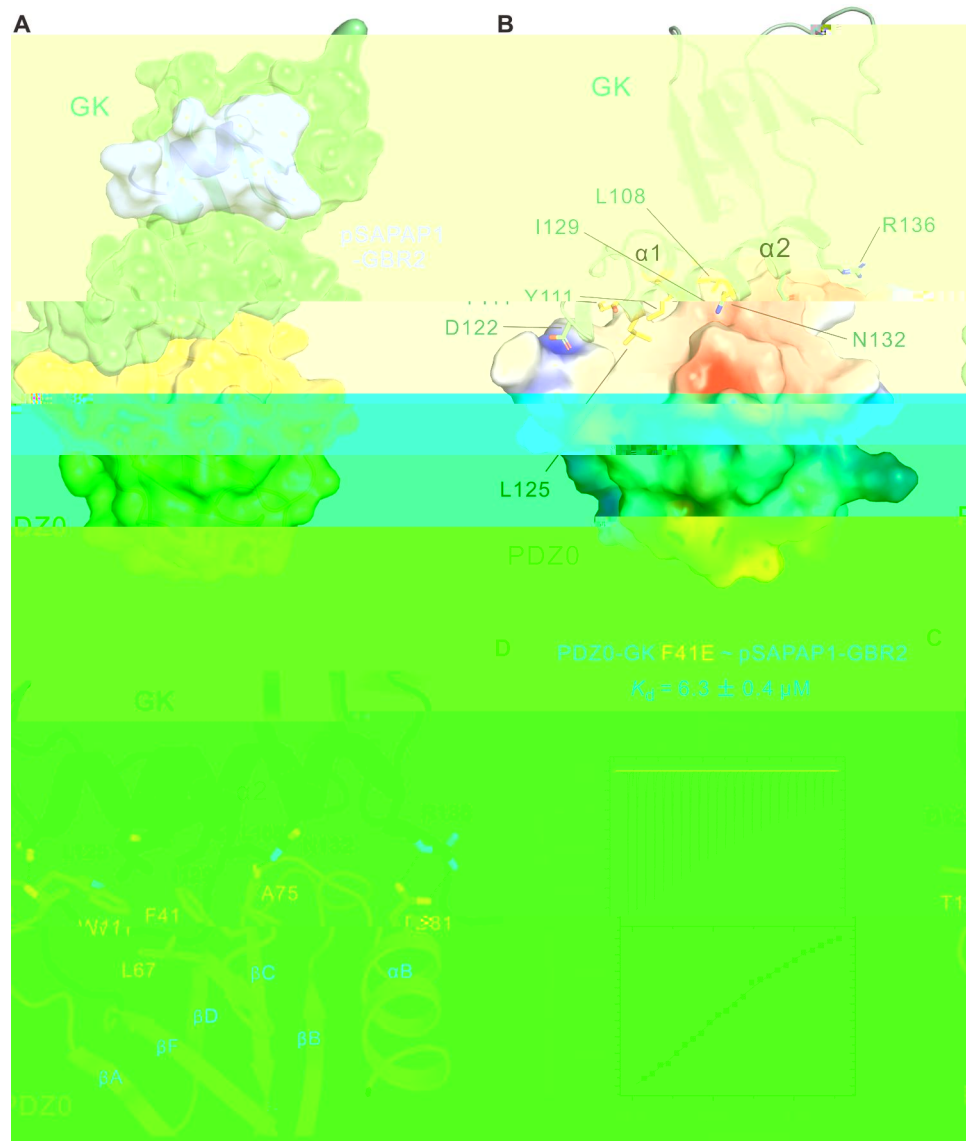


Fig. 3. The coupling interface between the PDZ0 and GK domains. (A) Combined surface and ribbon representations of the PDZ0-GK tandem. (B) Combined electrostatic surface and ribbon representations of the PDZ0-GK tandem showing an extensive hydrophobic contact between PDZ0 and $\alpha 1/\alpha 2$ from GK. In the electrostatic surface model, red and blue colors indicate negatively and positively charged surfaces, respectively, while white color highlights the hydrophobic surface. The surface potential representation has charge levels from $-3kT/e$ (red) to $+3kT/e$ (blue). The electrostatic potential distribution was generated using the APBS program in PyMOL. (C) Detailed interface between the PDZ0 and GK domains of MAGI2. Dotted lines denote hydrogen bonds and salt bridge interactions. (D) ITC-based measurement of the binding affinity between the F41E mutant of MAGI2 PDZ0-GK and the pSAPAP1-GBR2 peptide.

substantially impaired its binding to pSAPAP1-GBR2 (K_d of $6.3 \mu\text{M}$) (Fig. 3D). These data indicated that the PDZ0 and GK domains of MAGI2 form a structural and functional supramodule that is essential for phosphopeptide recognition.

Residue preference profile of pSAPAP1-GBR2 for MAGI2 binding

To date, the SAPAP family is the only known binding partner of MAGI2 GK. We reasoned that if we could determine a common binding motif of MAGI2 GK, we would be able to identify its previously unidentified binding targets and explore their new functions. To this end, we set to evaluate the residue preference at

each position of pSAPAP1-GBR2 for PDZ0-GK binding (Fig. 4A and table S2). We only considered the residues from R(-3) to T(+5) of pSAPAP1-GBR2 in the following study because the residues outside of this sequence are missing in the complex structure and most likely not essential for the interaction (Fig. 2C).

Substitution of R(-3) with Ala or even Lys led to a marked decreased binding affinity (Fig. 4A), suggesting that the position (-3) exclusively prefers the Arg residue. At the position (-2), substitution of R(-2) with small polar residues such as Asn or Ser did not change the affinity much, while replacement of R(-2) with Pro, Gly, Glu, or Val resulted in obvious decreased affinities (Fig. 4A). Of note, the R-2A mutant displayed a submicromolar affinity

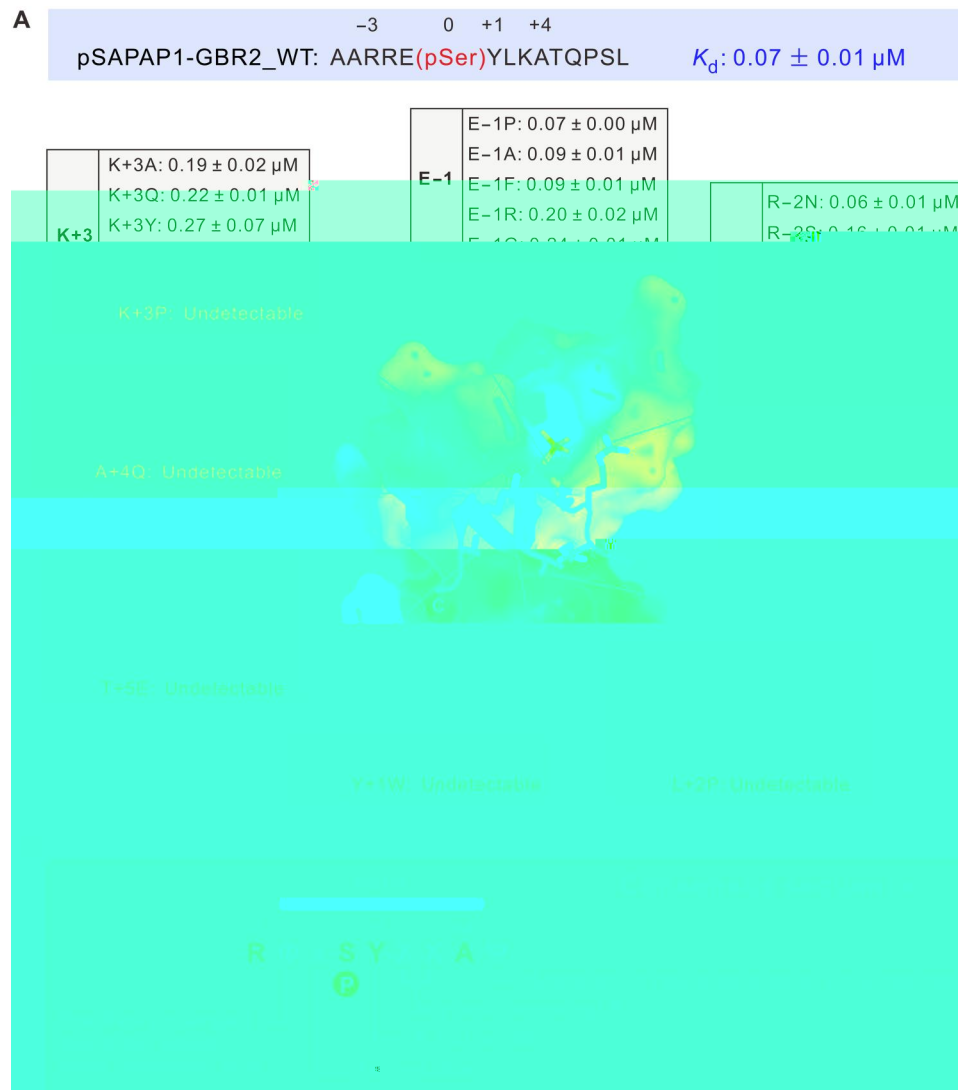


Fig. 4. A consensus phosphorylation-dependent motif for MAGI2 PDZ0-GK. (A) Summary of ITC-based measurements of the binding affinities between MAGI2 PDZ0-GK and various mutants of the pSAPAP1-GBR2 peptide showing the residue preference at each position of pSAPAP1-GBR2. In the electrostatic surface model, red and blue colors indicate negatively and positively charged surfaces, respectively, while white color highlights the hydrophobic surface. The surface potential representation has charge levels from $-3\text{kT}/e$ (red) to $+3\text{kT}/e$ (blue). The electrostatic potential distribution was generated using the APBS program in PyMOL. (B) Consensus MAGI2 PDZ0-GK binding motif: $-R-\Phi-x-S-Y-X-X-A-\Psi-$ (Φ : positively charged residues, small polar residues, or Ala; Ψ : hydrophobic residues or small polar residues; x : any residue; X : any residue except Pro).

(Fig. 4A), indicating that Ala is also allowed at this position. Mutating E(−1) to the residues with different properties did not affect the interaction, which suggests that the position (−1) could accommodate any residue (Fig. 4A). Y(+1) forms both hydrophobic and hydrogen-bonding interactions with MAGI2 PDZ0-GK (Fig. 2C). Although Phe displays the similar hydrophobicity to Tyr, the Y+1F mutant showed a 10-fold decreased affinity toward PDZ0-GK (Fig. 4A), most likely due to disruption of the hydrogen-bonding interactions. Intriguingly, the Y+1W mutant totally abolished the interaction (Fig. 4A), probably because its bulky side chain (i.e., indole ring) could not be accommodated by the hydrophobic groove on GK. Given that A(+4) inserts into the shallow hydrophobic groove of GK, one would expect that other hydrophobic residues would also fit well in this pocket. However, to our surprise, even

substitution of A(+4) with Val, which has the smallest hydrophobic side chain, led to a nearly 285-fold decreased binding affinity. Substitution of A(+4) with Ser, which has a similar side-chain size with Ala, also notably decreased the affinity (Fig. 4A). Moreover, the interaction was impaired when A(+4) was replaced by Gly, most likely due to disruption of the helical structure of the phosphopeptide. These results imply that the position (+4) may only favor the Ala residue. The residues at the positions (+2) and (+3) are not responsible for the binding as they are exposed to the solvent. Consistently, substitution of the residues at the two positions with any residue, except Pro, had no effect on the interaction (Fig. 4A). The introduction of Pro at the positions (+2) and (+3) would disfavor the formation of the helical structure of the phosphopeptide, which would not allow Y(+1) and A(+4) to insert into the hydrophobic groove on

GK. Last, at the position (+5), we concluded that hydrophobic residues are favorable, and small polar residues such as Asn may be accommodated as well, while charged residues are not preferred (Fig. 4A). On the basis of these results, we could delineate a consensus MAGI2 PDZ0-GK binding motif: -R-Φ-x-S-Y-X-X-A-Ψ- (Φ: positively charged residues, small polar residues, or Ala; Ψ: hydrophobic residues or small polar residues; x: any residue; X: any residue except Pro) (Fig. 4B).

Identification of previously unknown binding partners of MAGI2 PDZ0-GK

We next searched the Swiss-Prot database to find other human proteins that might use the consensus binding motif identified earlier to interact with MAGI2 PDZ0-GK. The searching results were further narrowed down by excluding the proteins where the motif is involved in a folded domain. To further increase the search stringency, we only selected target proteins whose motifs are highly conserved among human, mouse, rat, chicken, frog, and zebrafish. Using these criteria, we obtained several potential targets including Ephexin4 (also known as ARHGEF16), SGEF (also known as ARHGEF26), ARHGAP21, ARHGAP23, FRMD4A, INCENP, LL5A, and PROX1 (Fig. 5A and fig. S4). Many of these proteins are Rho GTPase regulatory factors, and others are scaffold proteins or transcription factors. They are involved in cell polarity, cell adhesion, cell migration, and cell division and are implicated in cancers and neurological diseases. As expected, the SAPAP family proteins emerge in this list as well (Fig. 5A).

To verify the search results, we synthesized four phosphorylated peptides of these potential targets and examined their bindings to MAGI2 PDZ0-GK. We found that these phosphorylated peptides (i.e., pEphexin4, pSGEF, pARHGAP23, and pLL5A) exhibited comparable affinities to MAGI2 PDZ0-GK, with K_d values of 0.23, 0.43, 0.27, and 0.33 μ M, respectively (Fig. 5, B to E). Therefore, we have identified a set of previously unknown MAGI2 PDZ0-GK binding targets.

Next, we wanted to know whether the binding mode used by MAGI2 PDZ0-GK to recognize these putative partners is similar to that of the MAGI2-SAPAP interaction. To this end, we tried to solve the structures of MAGI2 PDZ0-GK in complex with different phosphopeptides. We successfully determined two complex structures (i.e., the MAGI2-pSGEF and MAGI2-pEphexin4 complex) (fig. S5 and table S1). A direct comparison of these complex structures reveals that MAGI2 PDZ0-GK uses the same sites to recognize diverse phosphopeptides, and that the structural features of each complex interface are nearly identical (Fig. 5, F and G). The only difference is the residue at the position (-2) that coordinates the phosphate group of pSer⁰, which varies among the distinct phosphopeptides (Fig. 5, F and G).

Functional role of the MAGI2-SGEF complex in podocyte migration

Further, we set to explore the physiological functions of these MAGI2/phosphopeptide complexes. As mentioned above, the essential roles of MAGI2 in podocytes are manifested by the phenotypes of severe glomerular injury of both MAGI2-deficient mice and in patients with congenital nephrotic syndrome caused by mutations in *MAGI2*. Dysfunction of MAGI2-mediated signaling led to marked loss of actin cytoskeletal organization and decreased podocyte migration (26). We thus wanted to know whether the newly

identified MAGI2 partners are also involved in these processes and essential for normal podocyte function.

We first analyzed the expression of these genes in human cultured podocytes and found that SGEF was expressed in podocytes at both the transcript and protein levels (Fig. 6A and fig. S6). SGEF is a RhoG-specific GEF and has been reported to play crucial roles in the regulation of cell adhesion and cell migration (27, 28). However, SGEF has never been reported to function in podocytes. We hypothesized that if SGEF functions in the same pathway with MAGI2 in podocytes, down-regulation of SGEF would lead to podocyte dysfunction similar to that observed in MAGI2-deficient podocytes. We transduced a short hairpin RNA (shRNA) expression plasmid targeting SGEF into a conditionally immortalized human podocyte cell line and observed significantly reduced SGEF protein expression in the knockdown podocyte cell line compared with control podocytes transduced with a scrambled shRNA expression plasmid (Fig. 6, A and B). Knockdown of *SGEF* led to significantly reduced F-actin stress fibers in podocytes (Fig. 6, C and D) and marked reductions in migratory rate (Fig. 6, E and F), which is reminiscent of the behavior characteristics shared by *MAGI2* knockdown podocytes (26). These data suggested that SGEF might work together with MAGI2 in regulating podocyte migration.

To confirm the critical role of the MAGI2-SGEF interaction in podocyte migration, we conducted rescue experiments using SGEF wild type (WT) and two SGEF mutations (i.e., SGEF_S0A, a construct unable to be phosphorylated at Ser⁰; SGEF_delGBR, a construct lacking the entire GBR), which are expected to impair the MAGI2-SGEF interaction. Satisfyingly, the exogenous expression of SGEF_WT completely rescued the reduced migratory rate in *SGEF* knockdown podocytes, whereas neither SGEF_S0A nor SGEF_delGBR rescued the phenotype (Fig. 6, G and H). These results indicated that the MAGI2-SGEF interaction plays an essential role in cytoskeletal remodeling and cell migration in podocytes.

A non-phosphor inhibitory peptide capable of manipulating the MAGI2-SGEF signaling in podocytes

To further corroborate our findings, we aimed to develop an inhibitory peptide for MAGI2 PDZ0-GK and use it as a manipulating tool to dissect the MAGI2-SGEF signaling in podocytes. Although the phosphor-SGEF peptide is a readily effective tool, it may not be attractive for in vivo studies due to its susceptibility to dephosphorylation by cellular phosphatase(s). Thus, design of a non-phosphor inhibitory peptide would be a better strategy. Such a strategy has been successfully used in our previous study on the PSD-95-SAPAP complex in neuronal synapses (7). The non-phosphor inhibitory peptide (also known as the QSF peptide: RIRREEYR-RAINGQSF) occupies two sites on PSD-95 GK (Fig. 7A). While Site-1 on the GK domain of PSD-95 and MAGI2 are highly conserved (Fig. 2, C and D), Site-2 on the two GKs are largely different (Fig. 7, B and C). Site-2 of PSD-95 GK, a hydrophobic cradle formed by I593, A601 and L608, is occupied by the bulky hydrophobic side chain of F(+10) of the QSF peptide (Fig. 7B). However, Site-2 of MAGI2 GK contains polar residues such as E167 and S175 (Fig. 7C), which may favor positively charged residues. We thus reasonably speculated that substitution of F(+10) of the QSF peptide with Arg would ensure its binding to MAGI2 PDZ0-GK by forming potential polar interactions with E167 and S175 at Site-2.

Accordingly, several phosphomimicking MAGI2 GK inhibitory peptides were designed (i.e., the DSR, QSR, and QDR peptides) on

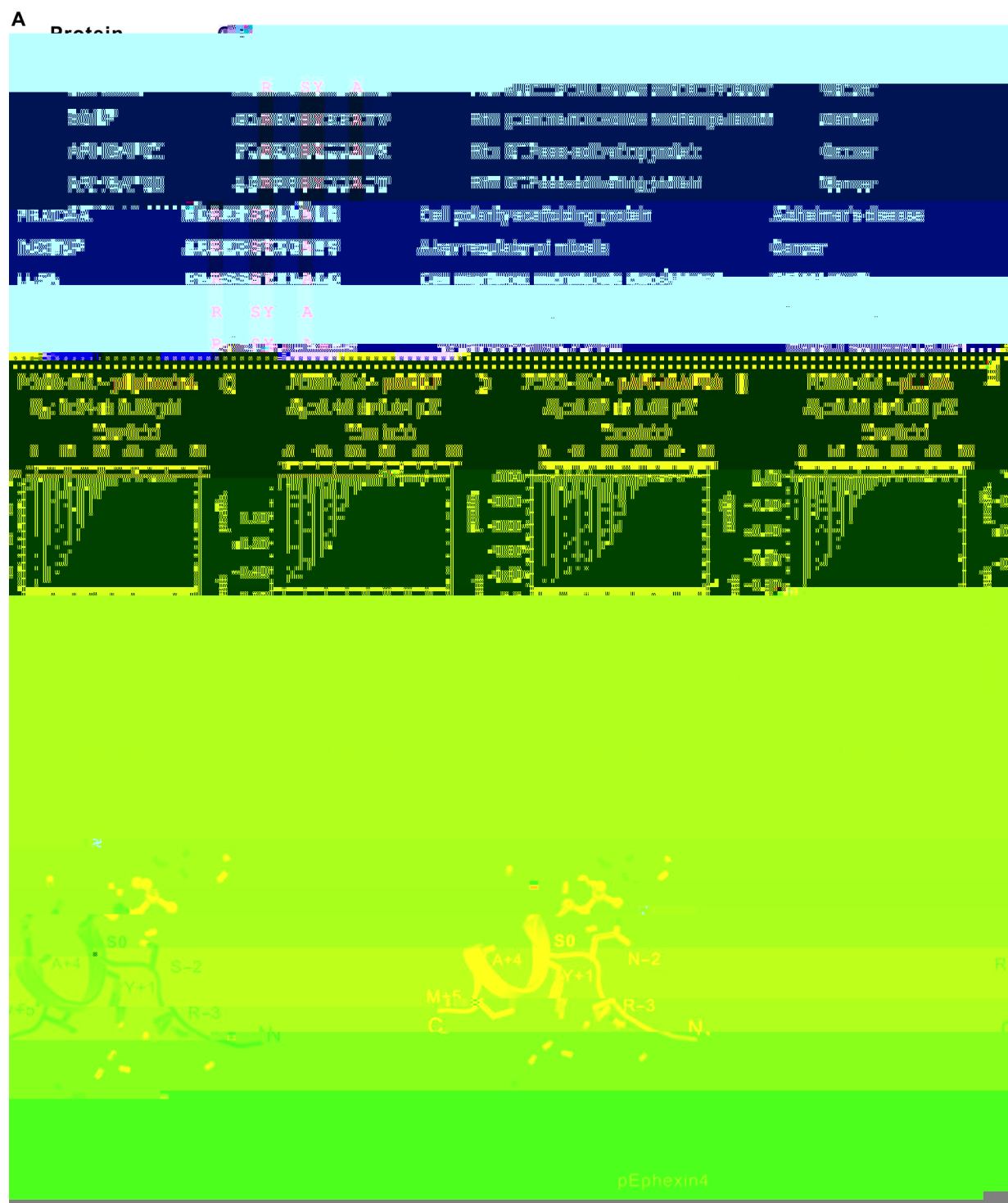
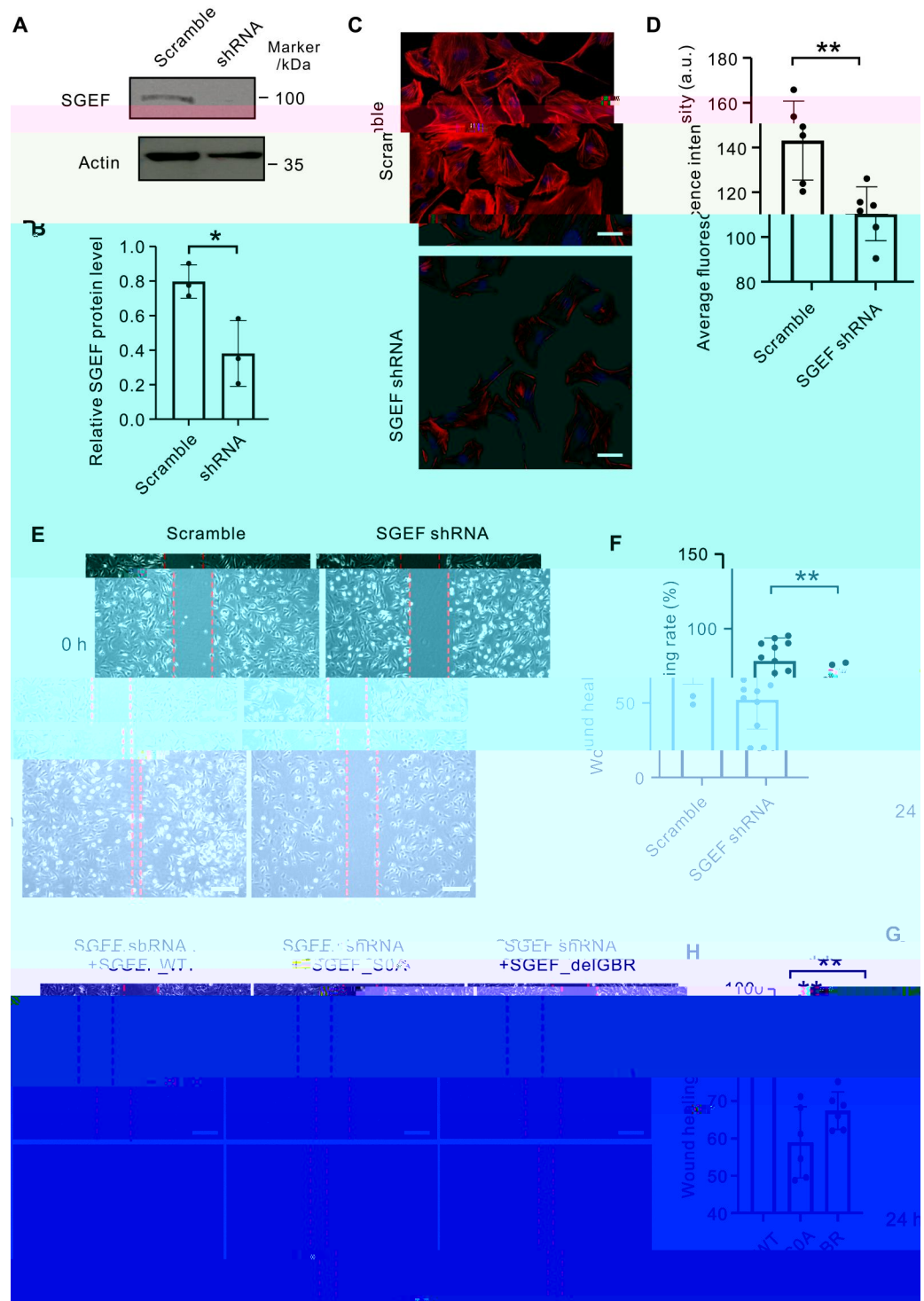


Fig. 5. Identification of previously unknown binding partners of MAGI2 PDZ0-GK. (A) Summary of the candidate binding partners of MAGI2 PDZ0-GK, with the consensus motif highlighted in orange. (B to E) ITC-based measurements of the binding affinities between MAGI2 PDZ0-GK and pEphexin4 (B), MAGI2 PDZ0-GK and pSGEF (C), MAGI2 PDZ0-GK and pARHGAP23 (D), and MAGI2 PDZ0-GK and pLL5A (E). (F and G) Detailed interface of the MAGI2 PDZ0-GK/pSGEF complex (F) and the MAGI2 PDZ0-GK/pEphexin4 complex (G). Dotted lines denote hydrogen bonds and electrostatic interactions.

Fig. 6. MAGI2-SGEF complex plays a role in podocyte migration. (A) Human cultured podocytes transduced with an shRNA expression plasmid targeting *SGEF* mRNA showed markedly reduced SGEF protein level compared with podocytes expressing a scrambled shRNA. (B) Quantification of the SGEF protein level from the experiments described in (A). * $P < 0.05$. $n = 3$ biologically independent samples. (C) Representative images showing knockdown of *SGEF* significantly reduced F-actin fibers in podocytes. F-actin filaments were stained by phalloidin. Scale bar, 50 μm . (D) Quantification of the average fluorescence intensities of actin fibers in (C). Data are presented as means \pm SEM from six fields ($n = 6$). ** $P < 0.01$. (E) Representative images showing that *SGEF* knockdown cells migrated more slowly than control cells. Scale bar, 200 μm . (F) Quantification of the wound healing rate from the results described in (E). The percent wound closure was quantified at fixed locations along the scratch. Data are presented as means \pm SEM from 11 fields ($n = 11$). ** $P < 0.01$. (G) Representative images showing that SGEF WT, but not SGEF_S0A or SGEF_delGBR, rescued the podocyte migratory rate. Scale bar, 200 μm . (H) Quantification of the wound healing rate from the results described in (G). Data are presented as means \pm SEM from six fields ($n = 6$). ** $P < 0.01$.



the basis of the sequence of the QSF peptide (Fig. 7D). ITC assays showed that these non-phosphor peptides bound to MAGI2 PDZ0-GK with K_d values ranging from 3.9 to 6.4 μM (Fig. 7, D and E). As anticipated, substitution of E(0) of the DSR peptide with Ala (referred to as DSR_E0A, this Glu residue mimics the phosphate group of the phosphopeptide) totally abolished its binding to MAGI2 PDZ0-GK (Fig. 7, D and E). Consistent with our peptide

design logic, substitution of R(+10)^{DSR} with Asp (i.e., the DSE peptide) markedly weakened the interaction, most likely due to the repulsive effect between E(+10)^{DSE} and E167 from Site-2 of MAGI2 GK (Fig. 7, D and E).

We next tried to evaluate the effect of the DSR peptide on the MAGI2-SGEF-mediated signaling in podocytes. To this end, the DSR_WT and DSR_E0A peptides were conjugated with a cell-

a conserved pocket for phosphopeptide binding. Decoupling the PDZ0-GK tandem substantially impairs the interaction, indicating that the PDZ0 domain mainly plays a structural role in stabilizing the GK domain. However, it cannot be ruled out that MAGI2 PDZ0 would recognize the as-yet-undefined PDZ-binding motif (PBM)-containing protein(s). A recent PDZ-PBM interactomics study may offer some valuable insights into this possibility (29). In this scenario, a more interesting question is whether binding of the PBM-containing protein(s) to PDZ0 would further regulate the interaction between MAGI2 GK and phosphopeptides. Structural analysis may provide some clues. It is noted that the $\beta\text{B}-\beta\text{C}$ loop of PDZ0 contacts directly with the GK domain (Fig. 2A). The $\beta\text{B}-\beta\text{C}$ loop of a PDZ domain is often involved in PDZ-PBM interaction (30). Therefore, one would reasonably envision that the binding of PBM at the $\beta\text{B}-\beta\text{C}$ loop of PDZ0 may induce a conformational rearrangement of the $\beta\text{B}-\beta\text{C}$ loop and then trigger an allosteric regulation of the GK/target interaction.

A perhaps more important discovery of this work is that, with the guidance of our biochemical and structural analyses, we could delineate a consensus MAGI2 PDZ0-GK binding motif: $-\text{R}-\Phi-\text{x}-\text{S}-\text{Y}-\text{X}-\text{X}-\text{A}-\Psi-$ (Fig. 4). Such a consensus sequence defines a set of previously unidentified partners of MAGI2 PDZ0-GK. Of particular interest, some of these partners are Rho GTPase regulatory proteins including GEFs and GTPase-activating proteins (GAPs). For example, SGEF and Ephexin4 are RhoG-specific GEFs (31, 32), whereas ARHGAP21 and ARHGAP23 are RhoGAPs (33). Rho GTPases are master regulators of cytoskeletal dynamics and involved in cell motility and cell adhesion (34). These results suggest that MAGIs may recruit diverse Rho GTPase regulatory proteins to orchestrate cytoskeletal dynamics in response to upstream signals. In support of this idea, we here demonstrate that the MAGI2-SGEF complex plays a role in regulating podocyte migratory rate. Similar scenarios may also occur in the MAGI2-mediated synaptic signaling. Neurons from MAGI2 α mutant mice exhibited elongated dendritic spines, which could be rescued by the expression of MAGI2 α , but not MAGI2 β that lacks the PDZ0-GK tandem (14). Such a defective spine morphology is mainly attributed to a significantly reduced amount of guanosine triphosphate (GTP)-bound RhoA, as the ectopic expression of the constitutively active RhoA shifts the spine length toward the normal level (14). These data strongly indicate that MAGI2 α , most likely via its PDZ0-GK, may recruit Rho GTPase regulatory proteins to fine-tune the activity of RhoA and consequently modulate the dendritic spine morphology. Future investigations are absolutely needed to verify this hypothesis.

It is worth noting that, since the phosphopeptide recognition pocket on the GK domain of both MAGI2 and PSD-95 are very similar (Fig. 2), one would expect that the consensus MAGI2 GK binding motif might also apply to PSD-95 GK. In other words, the newly identified partners of MAGI2 PDZ0-GK may interact with PSD-95 GK as well. PSD-95 GK bound to pEphexin4, pSGEF, pARHGAP23, and pLL5A as effectively as MAGI2 PDZ0-GK did (fig. S7). We previously demonstrated that PDZ domains of DLG1 (a close homolog of PSD-95) associate with and activate Ephexin4 RhoGEF to promote cell migration (32). A recent work reported that SGEF coordinates with DLG1 and Scribble to regulate the actomyosin-based contractility and barrier function at cell-cell junctions (35). The interaction between DLG1 and SGEF is mediated by the N-terminal region of SGEF (which covers the consensus

GBR sequence) and the GK domain of DLG1, although the underlying mechanism of the interaction remains unclear (35). Our current work provides a mechanistic basis for the assembly of the abovementioned DLG1-mediated complexes. The MAGI and DLG family proteins may bind to partner proteins with PBMs (e.g., Ephexin4 and SGEF; fig. S4) via both PDZ-PBM and GK-GBR interactions. These multivalent interactions would definitely drive the formation of large signaling complexes. The assembly of these signaling complexes could be spatiotemporally regulated by phosphorylation of GBR motifs of these partner proteins, providing an elegant regulatory mechanism for the MAGUK-mediated signaling pathways.

In summary, our biochemical, structural, cellular, and chemical biological data shed light on the target recognition mode for the cryptic GK domain of MAGIs. A highly conserved and widespread phosphorylation-dependent binding motif for both MAGI GKs and DLG GKs is delineated, which leads to the identification of a set of previously unknown binding partners of both proteins. We believe that many more GK-mediated regulatory functions are yet to be discovered in the future.

MATERIALS AND METHODS

Cloning, protein expression, and purification

Mouse *MAGI2* (GenBank: NM_001170746.1) and *MAGI1* (GenBank: NM_001029850.4) were amplified from a mouse brain complementary DNA (cDNA) library. Rat *MAGI3* (GenBank: NM_139084.2) and *DLG4* (encoding PSD-95, GenBank: NM_019621.1) were amplified from a rat brain cDNA library. Human *SGEF* gene (GenBank: BC078655.1) was provided by J. Han, Xiamen University, China. Various fragments of MAGIs and PSD-95 were cloned into a modified pET-32a vector (with thioredoxin-His₆-tag) or a modified pET-15b vector (with an N-terminal His₆-tag) as needed. WT or mutants of full-length SGEF were cloned into a pSF-Lenti vector (26) for rescue experiments. All of the mutations were generated by standard polymerase chain reaction (PCR)-based mutagenesis method using the Phanta Max superfidelity DNA polymerase (Vazyme Biotech Co. Ltd., catalog no. P505) and confirmed by DNA sequencing.

Recombinant proteins of MAGIs and PSD-95 were expressed in BL21 (DE3) *Escherichia coli* cells for 18 hours at 16°C induced by addition of isopropyl- β -D-thiogalactoside (IPTG) at a final concentration of 0.2 mM. The His₆-tagged proteins were purified using Ni²⁺-nitrilotriacetic acid agarose affinity chromatography (GE Healthcare, Cytiva) followed by Superdex-200 26/60 size exclusion chromatography (SEC) in the buffer containing 50 mM

with a time interval of 120 s to make sure that the titration peak returned to the baseline. In the ITC assays, the molar concentration of peptides and proteins was determined by NanoDrop (Thermo Fisher Scientific) according to the following equation: $c = A_{280\text{nm}}/\epsilon L$ (where $A_{280\text{nm}}$ is the absorbance at 280 nm, L is the path length, and ϵ is the molar extinction coefficient of proteins or peptides). The K_d values (\pm fitting error) were obtained from the data analysis using the Origin 7.0 software package (Microcal) by fitting the one-site binding model. Experiments were performed in triplicate, and one representative experiment was presented. The thermodynamic parameters (e.g., affinity, enthalpy, entropy, and stoichiometry) of all ITC assays were listed in table S2.

Crystallization and structure determination

For the reconstitution of the four MAGI2 PDZ0-GK/phosphopeptide complexes, the purified MAGI2 PDZ0-GK was mixed with four commercially synthesized phosphopeptides (GenScript), respectively, with a molar ratio of 1:1.2. All crystals were obtained by the sitting-drop vapor diffusion method at 16°C, with each drop composed of 0.5 μ l of protein complex (\sim 10 mg/ml) and 0.5 μ l of reservoir solution. The best crystals of MAGI2/pSAPAP1-GBR2 and MAGI2/pSAPAP1-GBR3 were yielded in 25% (w/v) PEG-3350 (polyethylene glycol, molecular weight 3350), 0.1 M Hepes (pH 7.5), 2.1 M ammonium phosphate dibasic, 0.2 M ammonium sulfate, and 0.1 M tris (pH 8.5). The best crystals of MAGI2/pEphexin4 and MAGI2/pSGEF were grown in 0.2 M magnesium chloride hexahydrate, 0.1 M tris (pH 8.5), 25% (w/v) PEG-3350, 0.2 M sodium chloride, 0.1 M tris (pH 8.5), and 25% (w/v) PEG-3350. Crystals were cryoprotected by adding glycerol into the mother liquor to the final concentration of 25% (v/v) and quickly frozen into liquid nitrogen. Diffraction data were collected at the Shanghai Synchrotron Radiation Facility (China). To solve the complex structure of MAGI2/pSAPAP1-GBR2, we first obtained a partial solution by molecular replacement via Phaser in PHENIX (36), using the structure of the PDZ1 domain of PDZD7 [Protein Data Bank (PDB): 2EEH] as the first searching template and the GMP-binding subdomain in the PSD-95 GK/pSAPAP1-GBR2 complex structure (PDB: 5YPO) as the second searching template. This partial solution was then integrated via PHENIX Autobuild to get an initial model (36). Further model building and refinement were carried out using Coot (37) and PHENIX (36) alternately. The complex structures of MAGI2/pSAPAP1-GBR3, MAGI2/pEphexin4, and MAGI2/pSGEF were all solved by molecular replacement using the MAGI2/pSAPAP1-GBR2 structure as the searching template and were further refined as described above. The final refinement statistics of these complex structures were summarized in table S1. Structural diagrams were prepared by PyMOL.

Podocyte cell culture

Generation and propagation of established conditionally immortalized podocyte cell lines were performed as previously described (38). Briefly, podocytes were propagated on type I collagen-coated dishes at the permissive temperature (33°C) in RPMI medium supplied with 10% fetal bovine serum and 1% (v/v) insulin-transferrin-selenium (Gibco, USA). For differentiation, cells were shifted to the nonpermissive temperature (37°C) and cultured for at least 1 week to induce full differentiation. Podocytes between passages 9 and 20 were used in all experiments.

Lentiviral infection and production

Scrambled shRNA (TR30021) plasmid was purchased from OriGene, Rockville, MD, already cloned into the pGFP-C-shLenti backbone. Short hairpin sequences specific for human SGEF are as follows: forward, 5'-GATCGCAAGATTGTATATCTGTATCAA GAGTACAGATATACAATCTTGCTTTTTTTG-3'; reverse, 5'-CCG GCAAAAAAGCAAGATTGTATATCTGTACTCTTGATACAGA TATACAATCTTGC-3'. The shRNA sequences were also cloned into the pGFP-C-shLenti vector. All lentiviral preparations and infections were conducted as previously described (39). In brief, infections were done at the permissive temperature in conditionally immortalized human podocytes, and then stable cell lines were established by selection with puromycin at a concentration of 2 μ g/ml. Knockdown and control transduced cell lines were grown at 37°C for at least 1 week before further experiments.

Wound healing assays

Differentiated mouse podocytes treated with indicated plasmids or TAT peptides were plated to complete confluence on type I collagen-coated six-well plates. A scratch was created using a 200- μ l sterile pipette. Loosely adherent cells were removed by washing with phosphate-buffered saline (PBS). Podocytes were imaged at several fixed locations along the scratch using a microscope immediately after wound creation (0 hours) and then returned to growth restrictive conditions for 24 hours before final imaging of wound healing. Percent wound healing rate was calculated using ImageJ processing program.

Immuno uorescent staining

Podocyte cells treated with indicated plasmids were seeded on 12-mm glass coverslips precoated with type I collagen in a 24-well cluster plate. Cells were then washed twice with PBS buffer, fixed in 4% paraformaldehyde in PBS for 10 min, and incubated with 0.1% Triton X-100 in PBS to increase permeability for 5 min. Cells were then incubated with phalloidin-iFluor 594 conjugate to stain F-actin (Abcam, USA) for 30 min at room temperature. Images were captured with a confocal microscope (LSM 880, Carl Zeiss, Germany). The average intensity of phalloidin staining was calculated using ImageJ processing program.

Quantitative PCR

The mRNA level of SGEF was assayed *in vitro* by real-time PCR (Applied Biosystems, USA). Amplification curves were analyzed using automated 7500 software platform, via the $\Delta\Delta C_T$ method. Human 18S ribosomal RNA (rRNA) was used as the endogenous control. The sequences of the primers were as follows: SGEF (f1) forward, AGCAACAGCATAACCCCTTTG; SGEF (f1) reverse, C TCCACCGGAAATCCGTAA; SGEF (f2) forward, ACAGCAGG ACGGTACATAGGA; SGEF (f2) reverse, CGTCGAAGTCGA GGAGAGG; 18S rRNA forward, GTAACCCGTTGAACCCATT ; 18S rRNA reverse, CCATCCAATCGGTAGTAGCG.

Western blot

Podocytes were lysed with radioimmunoprecipitation assay (RIPA) lysis buffer complemented with a protease inhibitor cocktail and tyrosine and serine-threonine phosphorylation inhibitors (Roche). The cell lysates were subjected to Western blot analysis using the following specific antibodies: anti-SGEF (#22183-1-AP, 1:500

dilution; Proteintech) and anti- β -actin (#4970s, 1:2000 dilution; Cell Signaling Technology).

Statistical analyses

All experiments were performed at least three times. All results are presented as means \pm SEM using the two-tailed Student's *t* test. All statistics were described in the figure legends. GraphPad Prism was used to compare the data between different groups.

Supplementary Materials

This PDF file includes:

Figs. S1 to S7

Tables S1 and S2

[View/request a protocol for this paper from Bio-protocol.](#)

REFERENCE AND NOTES

1. F. Ye, M. Zeng, M. Zhang, Mechanisms of MAGUK-mediated cellular junctional complex organization. *Curr. Opin. Struct. Biol.* **48**, 6–15 (2018).
2. J. Zhu, Y. Shang, M. Zhang, Mechanistic basis of MAGUK-organized complexes in synaptic development and signalling. *Nat. Rev. Neurosci.* **17**, 209–223 (2016).
3. J. M. Anderson, Cell signalling: MAGUK magic. *Curr. Biol.* **6**, 382–384 (1996).
4. A. J. W. te Velthuis, J. F. Admiraal, C. P. Bagowski, Molecular evolution of the MAGUK family in metazoan genomes. *BMC Evol. Biol.* **7**, 129 (2007).
5. J. Zhu, Y. Shang, C. Xia, W. Wang, W. Wen, M. Zhang, Guanylate kinase domains of the MAGUK family scaffold proteins as specific phospho-protein-binding modules. *EMBO J.* **30**, 4986–4997 (2011).
6. J. Zhu, Y. Shang, Q. Wan, Y. Xia, J. Chen, Q. Du, M. Zhang, Phosphorylation-dependent interaction between tumor suppressors Dlg and Lgl. *Cell Res.* **24**, 451–463 (2014).
7. J. Zhu, Q. Zhou, Y. Shang, H. Li, M. Peng, X. Ke, Z. Weng, R. Zhang, X. Huang, S. S. C. Li, G. Feng, Y. Lu, M. Zhang, Synaptic targeting and function of SAPAPs mediated by phosphorylation-dependent binding to PSD-95 MAGUKs. *Cell Rep.* **21**, 3781–3793 (2017).
8. S. Nagashima, M. Kodaka, H. Iwasa, Y. Hata, MAGI2/S-SCAM outside brain. *J. Biochem.* **157**, 177–184 (2015).
9. E. Danielson, N. Zhang, J. Metallo, K. Kaleka, S. M. Shin, N. Gerges, S. H. Lee, S-SCAM/MAGI-2 is an essential synaptic scaffolding molecule for the GluA2-containing maintenance pool of AMPA receptors. *J. Neurosci.* **32**, 6967–6980 (2012).
10. L. Kotelevets, E. Chastre, A new story of the three magi: Scaffolding proteins and lncRNA suppressors of cancer. *Cancers (Basel)* **13**, 4264 (2021).
11. N. Zhang, P. Zhong, S. M. Shin, J. Metallo, E. Danielson, C. M. Olsen, Q. S. Liu, S. H. Lee, S-SCAM, a rare copy number variation gene, induces schizophrenia-related endophenotypes in transgenic mouse model. *J. Neurosci.* **35**, 1892–1904 (2015).
12. E. A. Yemni, D. Monies, T. Alkhairallah, S. Bohlega, M. Abouelhoda, A. Magrashi, A. Mustafa, B. AlAbdulaziz, M. Alhamed, B. Baz, E. Goljan, R. Albar, A. Jabaan, T. Faquih, S. Subhani, W. Ali, J. Shinwari, B. Al-Mubarak, N. Al-Tassan, Integrated analysis of whole exome sequencing and copy number evaluation in Parkinson's disease. *Sci. Rep.* **9**, 3344 (2019).
13. K. Hirao, Y. Hata, I. Yao, M. Deguchi, H. Kawabe, A. Mizoguchi, Y. Takai, Three isoforms of synaptic scaffolding molecule and their characterization. Multimerization between the isoforms and their interaction with N-methyl-D-aspartate receptors and SAP90/PSD-95-associated protein. *J. Biol. Chem.* **275**, 2966–2972 (2000).
14. J. Iida, H. Ishizaki, M. Okamoto-Tanaka, A. Kawata, K. Sumita, S. Ohgake, Y. Sato, H. Yorifuji, N. Nukina, K. Ohashi, K. Mizuno, T. Tsutsumi, A. Mizoguchi, J. Miyoshi, Y. Takai, Y. Hata, Synaptic scaffolding molecule alpha is a scaffold to mediate N-methyl-D-aspartate receptor-dependent RhoA activation in dendrites. *Mol. Cell. Biol.* **27**, 4388–4405 (2007).
15. K. Hirao, Y. Hata, N. Ide, M. Takeuchi, M. Irie, I. Yao, M. Deguchi, A. Toyoda, T. C. Sudhof, Y. Takai, A novel multiple PDZ domain-containing molecule interacting with N-methyl-D-aspartate receptors and neuronal cell adhesion proteins. *J. Biol. Chem.* **273**, 21105–21110 (1998).
16. A. H. Rasmussen, H. B. Rasmussen, A. Silahtaroglu, The DLGAP family: Neuronal expression, function and role in brain disorders. *Mol. Brain* **10**, 43 (2017).
17. M. Zeng, Y. Shang, T. Guo, Q. He, W. H. Yung, K. Liu, M. Zhang, A binding site outside the canonical PDZ domain determines the specific interaction between Shank and SAPAP and their function. *Proc. Natl. Acad. Sci. U.S.A.* **113**, E3081–E3090 (2016).
18. J. M. Welch, J. Lu, R. M. Rodriguez, N. C. Trotta, J. Peca, J. D. Ding, C. Feliciano, M. Chen, J. P. Adams, J. Luo, S. M. Dudek, R. J. Weinberg, N. Calakos, W. C. Wetsel, G. Feng, Corticostriatal synaptic defects and OCD-like behaviours in Sapap3-mutant mice. *Nature* **448**, 894–900 (2007).
19. S. Lehtonen, J. J. Ryan, K. Kudlicka, N. Iino, H. Zhou, M. G. Farquhar, Cell junction-associated proteins IQGAP1, MAGI-2, CASK, spectrins, and alpha-actinin are components of the nephrin multiprotein complex. *Proc. Natl. Acad. Sci. U.S.A.* **102**, 9814–9819 (2005).
20. K. Ihara, K. Asanuma, T. Fukuda, S. Ohwada, M. Yoshida, K. Nishimori, MAGI-2 is critical for the formation and maintenance of the glomerular filtration barrier in mouse kidney. *Am. J. Pathol.* **184**, 2699–2708 (2014).
21. H. Yamada, N. Shirata, S. Makino, T. Miyake, J. A. O. Trejo, K. Yamamoto-Nonaka, M. Kikyo, M. A. Empitu, I. N. Kadariswantiningsih, M. Kimura, K. Ichimura, H. Yokoi, M. Mukoyama, A. Hotta, K. Nishimori, M. Yanagita, K. Asanuma, MAGI-2 orchestrates the localization of backbone proteins in the slit diaphragm of podocytes. *Kidney Int.* **99**, 382–395 (2021).
22. H. Zhang, L. Lin, J. Liu, L. Pan, Z. Lin, M. Zhang, J. Zhang, Y. Cao, J. Zhu, R. Zhang, Phase separation of MAGI2-mediated complex underlies formation of slit diaphragm complex in glomerular filtration barrier. *J. Am. Soc. Nephrol.* **32**, 1946–1960 (2021).
23. N. Shirata, K. I. Ihara, K. Yamamoto-Nonaka, T. Seki, S. I. Makino, J. A. Oliva Trejo, T. Miyake, H. Yamada, K. N. Campbell, T. Nakagawa, K. Mori, M. Yanagita, P. Mundel, K. Nishimori, K. Asanuma, Glomerulosclerosis induced by deficiency of membrane-associated guanylate kinase inverted 2 in kidney podocytes. *J. Am. Soc. Nephrol.* **28**, 2654–2669 (2017).
24. A. Bierzynska, K. Soderquest, P. Dean, E. Colby, R. Rollason, C. Jones, C. D. Inward, H. J. McCarthy, M. A. Simpson, G. M. Lord, M. Williams, G. I. Welsh, A. B. Koziell, M. A. Saleem; on behalf of NephroS, the UK study of Nephrotic Syndrome, MAGI2 mutations cause congenital nephrotic syndrome. *J. Am. Soc. Nephrol.* **28**, 1614–1621 (2017).
25. S. Ashraf, H. Kudo, J. Rao, A. Kikuchi, E. Widmeier, J. A. Lawson, W. Tan, T. Hermle, J. K. Warejko, S. Shril, M. Airik, T. Jobst-Schwan, S. Lovric, D. A. Braun, H. Y. Gee, D. Schapiro, A. J. Majmundar, C. E. Sadowski, W. L. Pabst, A. Daga, A. T. van der Ven, J. M. Schmidt, B. C. Low, A. B. Gupta, B. K. Tripathi, J. Wong, K. Campbell, K. Metcalfe, D. Schanze, T. Niihori, H. Kaito, K. Nozu, H. Tsukaguchi, R. Tanaka, K. Hamahira, Y. Kobayashi, T. Takizawa, R. Funayama, K. Nakayama, Y. Aoki, N. Kumagai, K. Iijima, H. Fehrenbach, J. A. Kari, S. El Desoky, S. Jalalah, R. Bogdanovic, N. Stajic, H. Zappel, A. Rakhmetova, S. R. Wassmer, T. Jckel

- comprehensive Python-based system for macromolecular structure solution. *Acta Crystallogr. D Biol. Crystallogr.* **66**, 213–221 (2010).
37. P. Emsley, K. Cowtan, Coot: Model-building tools for molecular graphics. *Acta Crystallogr. D Biol. Crystallogr.* **60**, 2126–2132 (2004).
38. M. A. Saleem, M. J. O'Hare, J. Reiser, R. J. Coward, C. D. Inward, T. Farren, C. Y. Xing, L. Ni, P. W. Mathieson, P. Mundel, A conditionally immortalized human podocyte cell line demonstrating nephrin and podocin expression. *J. Am. Soc. Nephrol.* **13**, 630–638 (2002).
39. M. Husain, G. L. Gusella, M. E. Klotman, I. H. Gelman, M. D. Ross, E. J. Schwartz, A. Cara, P. E. Klotman, HIV-1 Nef induces proliferation and anchorage-independent growth in podocytes. *J. Am. Soc. Nephrol.* **13**, 1806–1815 (2002).
40. G. E. Crooks, G. Hon, J. M. Chandonia, S. E. Brenner, WebLogo: A sequence logo generator. *Genome Res.* **14**, 1188–1190 (2004).

Acknowledgments: We thank beamlines BL02U1, BL18U1, and BL19U1 at Shanghai Synchrotron Radiation Facility (SSRF, China) for x-ray beam time and the staff members of the Large-scale Protein Preparation System and Molecular Imaging System at the National Facility for Protein Science in Shanghai (NFPS), Shanghai Advanced Research Institute, Chinese Academy of Sciences, China for providing technical support and assistance in data collection and analysis. **Funding:** This work was supported by a grant from the National Science and Technology Innovation 2030—Major Projects (2022ZD0214400) to J.Z., grants from the National Natural Science Foundation of China (32122036, U2032122, and 31770779) to J.Z., a grant from the Science and Technology Commission of Shanghai Municipality (20S11900200), a

grant from the Interdisciplinary Innovative Talent Training Program of Shanghai Jiao Tong University to J.Z., a grant from the National Key R&D Program of China (2018YFA0507900) to J.Z., a grant from the Scientific Research Foundation for Youth Scholars of Shanghai Jiao Tong University (AF0890029) to L.L., a grant from the Shanghai Pujiang Program (21PJ1412400) to A.C., a grant from the Shanghai Sixth People's Hospital affiliated to Shanghai Jiao Tong University School of Medicine (ynms202205) to A.C., and a grant from the Clinical Specialty of Shanghai Putuo District Health System (2021tszk02) to A.C. **Author contributions:** Meng Zhang, A.C., J.Z., and Mingjie Zhang conceived the study. Meng Zhang and L.L. performed the biochemical and structural experiments. Y.S. provided technical support and assistance in structure determination and analysis. Y.C. and A.C. performed podocyte-related experiments. All authors analyzed the data. J.Z. wrote the manuscript with input from all authors. J.Z. coordinated the project. **Competing interests:** The authors declare that they have no competing interests. **Data and materials availability:** All data needed to evaluate the conclusions in the paper are present in the paper and/or the Supplementary Materials. The atomic coordinates of the MAGI2/pSAPAP1-GBR2, MAGI2/pSAPAP1-GBR3, MAGI2/pEphexin4, and MAGI2/pSGEF complex have been deposited to the PDB under the accession codes 7YKH, 7YKI, 7YKF, and 7YKG, respectively.

Submitted 14 October 2022

Accepted 7 April 2023

Published 10 May 2023

10.1126/sciadv.adf3295

Phosphorylation-dependent recognition of diverse protein targets by the cryptic GK domain of MAGI MAGUKs

Meng Zhang, Aili Cao, Lin Lin, Ying Chen, Yuan Shang, Chao Wang, Mingjie Zhang, and Jinwei Zhu

Sci. Adv., **9** (19), eadf3295.
DOI: 10.1126/sciadv.adf3295

View the article online

<https://www.science.org/doi/10.1126/sciadv.adf3295>

Permissions

<https://www.science.org/help/reprints-and-permissions>

Use of this article is subject to the [Terms of service](#)

Science Advances (ISSN) is published by the American Association for the Advancement of Science. 1200 New York Avenue NW, Washington, DC 20005. The title *Science Advances* is a registered trademark of AAAS.
Copyright © 2023 The Authors, some rights reserved; exclusive licensee American Association for the Advancement of Science. No claim to original U.S. Government Works. Distributed under a Creative Commons Attribution NonCommercial License 4.0 (CC BY-NC).